4-1987

M2 Tidal Currents in the Eastern Equatorial Pacific Ocean

Robert H. Weisberg
University of South Florida, weisberg@marine.usf.edu

D. Halpern
California Institute of Technology

T. Y. Tang
University of South Florida

S. M. Hwang
University of Miami

JOURNAL OF GEOPHYSICAL RESEARCH, VOL. 92, NO. C4, PAGES 3821-3826, APRIL 15, 1987

M_2 Tidal Currents in the Eastern Equatorial Pacific Ocean

R. H. WEISBERG,[1] D. HALPERN,[2] T. Y. TANG,[1] AND S. M. HWANG[3]

Current meter measurements recorded over the water column at 10 depths ranging from 20 m to 3027 m using surface and subsurface moorings near 0°, 110°W are analyzed for the M_2 tidal current over a 10-month sampling interval. A kinematical description is given by month and depth, followed by a decomposition into a barotropic mode and three baroclinic modes. The barotropic tide was dominant, and its hodograph was stable over the 10 months sampled. The baroclinic tide was random, isotropic, and without mode preference.

1. INTRODUCTION

During part of the National Oceanic and Atmospheric Administration (NOAA) Equatorial Pacific Ocean Climate Studies (EPOCS) program, moored current meters were maintained over the entire water column near 0°, 110°W for a 10-month period beginning March 30, 1980. While these measurements were principally aimed at monitoring the low-frequency variability associated with climate, they also presented an opportunity for studying deep ocean tidal currents in a region previously unexamined for such purposes. This paper focuses upon the M_2 tidal current distribution over the water column and its description in terms of barotropic and baroclinic modes.

A review of ocean tides is given by *Hendershott* [1981]. Very few empirical studies of open ocean tidal currents exist owing to a lack of data. Of these, only a smaller subset have had sufficient data over the water column to separate the barotropic and baroclinic modes. Such analyses are presented for the North Atlantic Ocean by *Schott and Willebrand* [1973], *Gould and McKee* [1973], *Magaard and McKee* [1973], and *Hendry* [1977], and some additional studies have been performed on data from marginal seas. Similar studies are not available for the tropical Pacific Ocean. The region closest to the present study area in the Pacific Ocean where tidal current analyses have been performed [*Munk et al.*, 1970] is adjacent to the southern California coast.

Global numerical solutions to the Laplace tidal equations are reviewed by *Hendershott* [1975, 1981]. Of the models presented, the one by *Pekeris and Accad* [1969] provides a global chart of M_2 tidal current ellipses. This along with the recent tidal model of *Schwiderski* [1980] provide a basis for comparison with the analyses to be presented here. The addition of such points for comparison is necessary for the confirmation and improvement of the global tidal maps which are also important for geophysics and geodesics studies.

The paper will proceed as follows. Section 2 discusses the field data collection effort and describes the kinematics of the M_2 tidal current variations in time and depth. A dynamical mode decomposition based upon the observed buoyancy frequency profile and a data projection onto the barotropic and the first three baroclinic modes will be given in section 3 along with an error analysis for the barotropic tidal current ellipse based upon the observed variability over the 10 months of data. Section 4 then summarizes and discusses the findings.

2. FIELD PROGRAM AND DATA

Horizontal velocity measurements were made at 10 depths for 10 months in the eastern equatorial Pacific Ocean near 0°, 110°W using both surface and subsurface moored current meters. Data at 20 m, 50 m, and 100 m were recorded by vector-averaging current meters (VACMs) suspended beneath a tautly moored surface-following buoy, and data at 277 m, 727 m, 927 m, 1027 m, 2027 m, 2127 m, and 3027 m were recorded by Aanderaa RCM4 current meters (with the exception of the 277-m instrument, which was a VACM) suspended beneath a subsurface buoy at 275 m. Both moorings were within 2 km of the equator, with the surface mooring 80 km to the east of the subsurface mooring, as is shown in Figure 1. Intercomparison tests between VACMs with RCM4s by *Halpern and Pillsbury* [1976] have shown that while there are subtle differences between the responses of these instruments at the M_2 frequency, these differences are not large enough to bias the results presented here.

The vertical distributions of the north and east velocity component means and standard deviations over the 10-month sampling interval are shown in Figure 2, along with a buoyancy frequency profile obtained by averaging several deep conductivity-temperature-depth (CTD) casts from the study area in July 1979 (S. P. Hayes, personal communication, 1985). The background currents consist of the surface westward flowing South Equatorial Current, the subsurface eastward flowing Equatorial Undercurrent between approximately 30 m and 250 m, and much smaller mean flows below. Subsurface mooring measurements (below 277 m) were therefore in regions of weak mean shear, and this, combined with pressure observations that showed intermittent and generally less than 5-m vertical mooring excursions, suggests that tidal current biasing by mooring motion in the presence of ambient shear was negligible. The buoyancy frequency profile shows a peak in the shallow thermocline and a secondary peak below the thermostad near the 277-m instrument depth. A relative maximum in baroclinic tidal current amplitude may therefore be expected at this depth.

To investigate the temporal and vertical variations of the M_2 tidal currents, the data were divided into 10 segments, each being 720 hours long, with the first one beginning on March 30, 1980, at 1200 UT. These segments were Fourier analyzed to compute hodograph ellipses with 2 degrees of

[1] Department of Marine Science, University of South Florida, Saint Petersburg.
[2] Jet Propulsion Laboratory, California Institute of Technology, Pasadena.
[3] Cooperative Institute for Marine and Atmospheric Studies, Rosenstiel School for Marine and Atmospheric Science, University of Miami, Florida.

Paper number 7C0078.
0148-0227/87/007C-0078$05.00

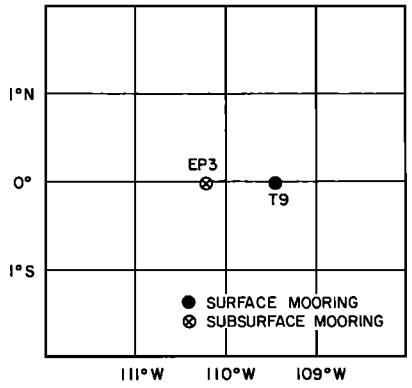

Fig. 1. Mooring locations.

freedom centered upon the M_2 tidal frequency. The results are shown in Figure 3, and the ellipse parameters of semimajor axis, semiminor axis, orientation, and temporal phase are given in Table 1. The sense of rotation is clockwise for all ellipses excepting the ones marked by a plus sign in the upper right corner. Anticlockwise rotation was limited to depths of 277 m and above. Temporal phase has been adjusted to represent the lag in hours between the lunar transit of the Greenwich meridian and the time of maximum current velocity. Below 277 m the tidal ellipses are uniform in time and depth, especially below 1027 m. At 277 m, while the ellipses are generally similar in shape to those below, the amplitudes tend to be larger. Above 277 m the variations from month to month tend to be the largest. Even so, there are months (e.g., September) when the M_2 tidal current ellipses are uniform over the entire water column. The phases show a similar degree of uniformity in time and depth, especially below 277 m. Given the uniformity of the ellipse parameters, it would appear that the M_2 tidal currents of this eastern equatorial Pacific Ocean location have a measureable barotropic mode.

3. Dynamical Modes

The analyses of the M_2 barotropic tidal current ellipse, its root-mean-squared (rms) error, and the residual baroclinic tidal current ellipses proceeded as follows. First, the dynamical modes associated with the buoyancy frequency profile of Figure 2 were calculated. Second, the M_2 tidal velocity component data were projected by month onto the barotropic and the first three baroclinic modes by minimizing the linear mean squared error, and these velocity components were then combined to compute ellipses for each of these modes by month. Third, the mean barotropic M_2 tidal current ellipse and its rms deviations over the 10-month sampling duration were calculated to estimate the error associated with the barotropic tidal current ellipse under the assumption that it should be time invariant. This uncertainty in the assumed deterministic barotropic tidal current ellipse provides a measure of the stochastic noise in the calculation which may then be compared with the baroclinic mode ellipses, which themselves are stochastic.

The dynamical modes were calculated by solving the verti-

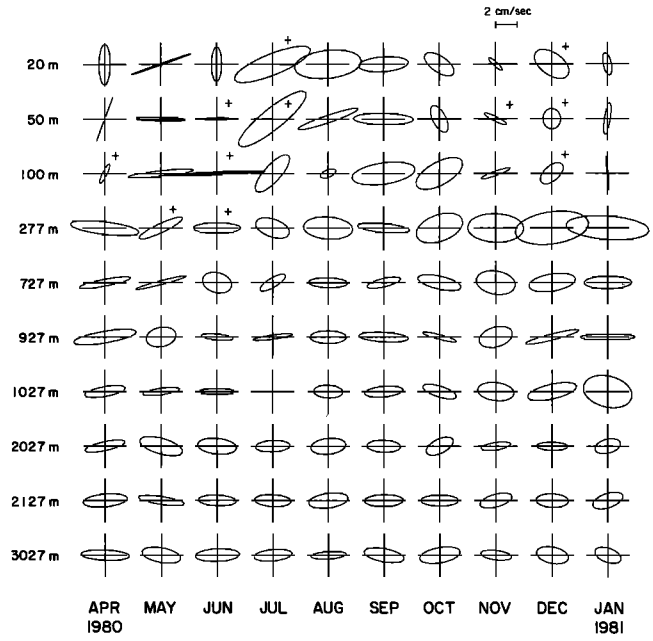

Fig. 3. M_2 tidal current ellipses by month at each of the 10 depths obtained from Fourier coefficients computed over a bandwidth of 1.39×10^{-3} centered upon the semidiurnal tidal frequency. With the exception of the ones noted by a plus sign, all of the ellipses are polarized clockwise.

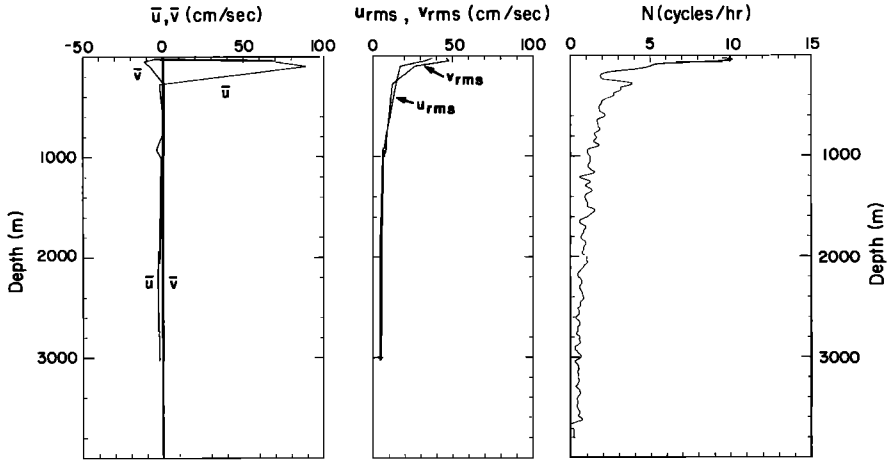

Fig. 2. Velocity component means and standard deviations averaged over the 10-month sampling interval beginning March 30, 1980, and a buoyancy frequency profile from the equator at 110°W obtained by averaging several CTD casts during July 1979 (S. P. Hayes, personal communication, 1985).

TABLE 1. M_2 Tidal Current Ellipse Parameters Computed by Month for Each of the 10 Depths Samples From 20 m to 3027 m

Depth, m	Parameter	April	May	June	July	Aug.	Sept.	Oct.	Nov.	Dec.	Jan.
20	semimajor	1.92	2.98	1.62	3.84	3.16	2.34	1.60	0.86	1.84	1.05
	semiminor	0.51	0.06	0.47	0.97	1.29	0.69	0.73	0.19	1.03	0.39
	orientation	1.56	0.33	1.56	0.38	0.11	0.07	−0.60	−0.75	−0.61	−1.34
	phase	7.22	7.29	2.92	6.31	6.44	6.26	5.98	4.67	10.48	10.04
50	semimajor	2.20	2.27	1.11	3.99	2.99	2.83	1.37	1.18	0.96	1.50
	semiminor	0.02	0.17	0.10	0.98	0.34	0.53	0.60	0.22	0.82	0.28
	orientation	1.21	−0.03	0.04	0.68	0.33	−0.02	−1.10	−0.46	−1.54	1.42
	phase	7.66	7.01	7.14	6.40	6.19	6.11	5.68	4.97	8.31	3.60
100	semimajor	1.01	3.05	4.24	2.26	0.78	3.00	2.41	1.43	1.30	1.57
	semiminor	0.21	0.25	0.06	0.77	0.34	0.99	1.07	0.21	0.70	0.04
	orientation	1.21	0.11	0.05	0.84	0.38	0.14	0.51	0.35	0.72	1.50
	phase	7.34	6.55	6.92	6.40	6.86	5.91	5.03	4.67	0.48	10.36
277	semimajor	3.23	2.23	2.22	1.66	2.33	2.47	2.26	2.60	3.46	3.93
	semiminor	0.58	0.41	0.48	0.83	1.02	0.41	1.22	1.32	1.48	1.08
	orientation	−0.12	0.44	0.00	−0.33	−0.07	−0.08	0.34	−0.03	0.14	−0.07
	phase	7.61	6.91	6.94	6.30	6.07	5.90	6.17	5.91	5.43	5.59
727	semimajor	2.43	2.44	1.40	1.39	1.86	1.61	2.05	1.82	2.19	2.25
	semiminor	0.31	0.17	0.93	0.43	0.45	0.39	0.60	1.08	0.79	0.58
	orientation	0.18	0.25	−0.27	0.54	−0.02	0.23	−0.23	−0.18	0.16	0.01
	phase	7.70	7.19	6.98	6.61	6.38	6.18	6.49	6.63	5.93	6.17
927	semimajor	2.97	1.41	1.51	1.90	1.72	2.34	1.62	1.59	2.55	2.59
	semiminor	0.54	0.90	0.27	0.18	0.58	0.44	0.22	0.91	0.28	0.27
	orientation	0.17	0.22	−0.09	0.14	−0.01	−0.06	−0.26	0.29	0.25	0.01
	phase	7.57	6.29	6.79	6.58	6.43	6.02	6.56	5.85	5.46	8.92
1027	semimajor	1.93	1.72	1.74	0.83	1.38	1.82	1.63	1.69	2.34	2.34
	semiminor	0.45	0.29	0.26	0.03	0.60	0.49	0.50	0.84	0.68	1.44
	orientation	0.18	0.14	0.00	0.04	−0.04	0.09	−0.31	−0.11	0.22	−0.24
	phase	7.48	7.22	7.00	6.57	6.68	6.10	7.16	7.27	6.67	7.83
2027	semimajor	1.92	2.05	1.83	1.64	1.66	1.60	1.37	1.39	1.46	1.25
	semiminor	0.41	0.72	0.73	0.53	0.73	0.56	0.65	0.34	0.38	0.64
	orientation	0.22	−0.28	−0.09	0.04	0.11	−0.03	0.47	0.15	−0.02	0.26
	phase	7.24	7.58	7.02	6.76	6.40	6.20	6.09	5.58	5.88	6.27
2127	semimajor	2.09	2.16	1.79	1.74	1.89	1.82	1.76	1.54	1.52	1.50
	semiminor	0.58	0.36	0.49	0.55	0.67	0.55	0.50	0.58	0.63	0.66
	orientation	0.10	−0.14	−0.04	−0.04	0.14	0.02	0.00	0.27	−0.03	0.32
	phase	7.36	7.30	6.93	6.75	6.40	6.07	6.07	5.52	6.43	5.53
3027	semimajor	2.27	1.84	2.09	1.80	1.68	1.90	1.92	1.44	1.52	1.30
	semiminor	0.47	0.68	0.58	0.52	0.33	0.61	0.70	0.44	0.76	0.66
	orientation	−0.04	−0.18	0.05	0.10	0.06	−0.18	0.18	−0.12	−0.20	−0.33
	phase	7.24	7.34	6.81	6.52	6.27	6.19	5.64	5.73	6.13	7.84

The units for semimajor and semiminor axis are centimeters per second, the unit for orientation is radians measured anticlockwise from east, and phase is in hours. The bandwidth used in the calculation was 1.389×10^{-3} c/h.

cal structure equation for the vertical velocity component:

$$F_n''(z) + \frac{N^2(z)}{C_n^2} F_n(z) = 0 \quad (1)$$

where $F_n(z)$ are the eigenfunctions for the nth mode, C_n are the eigenvalues, and $N(z)$ is the buoyancy frequency. The free surface boundary condition used to allow for a barotropic mode is

$$F_n'(0) - \frac{g}{C_n^2} F_n(0) = 0 \quad (2)$$

where g is the gravitational acceleration and the bottom boundary condition is $F_n = 0$. A finite difference calculation for the eigenvalues and the eigenfunctions was employed beginning at the surface and using a trial and error method to match the bottom boundary condition. The eigenfunctions for the vertical structure of the vertical velocity component were normalized and then differentiated to obtain the eigenfunctions proportional to the horizontal velocity components. The results for the barotropic and the first three baroclinic modes are shown in Figure 4, and the corresponding eigenvalues for these modes are given in Table 2. Since the eigenvalues are the phase speeds for the horizontal wave functions, the barolinic modes at the M_2 tidal frequency all have wavelengths comparable to or smaller than the 80-km separation between the surface and the subsurface moorings on which the measurements above 277 m and at 277 m and below were made, respectively. For this reason, only the subsurface mooring

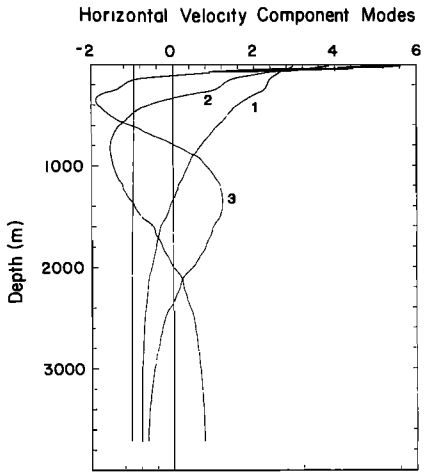

Fig. 4. Horizontal velocity component eigenfunctions for the barotropic and the first three baroclinic modes computed from the buoyancy frequency profile of Figure 2. The units are dimensionless, and amplitudes are obtained from the modal projections given in Figures 5*a* and 5*b*.

data at the seven depths between 277 m and 3027 m were used for the dynamical mode projections.

The dynamical mode projections for the tidal current velocity components were obtained by seeking a set of complex coefficients A_n which minimize the mean squared error between the complex Fourier coefficients of the data $a(z_i)$ and the linear combination of the barotropic mode and the first three baroclinic modes. The mean squared error ε is

$$\varepsilon = \sum_{i=1}^{7} \left\{ a(z_i) - \sum_{n=0}^{3} A_n F_n'(z_i) \right\} \left\{ a(z_i) - \sum_{n=0}^{3} A_n F_n'(z_i) \right\}^* \tag{3}$$

where the asterisk denotes the complex conjugate, $n = 0$ is the barotropic mode, and $n = 1, 2, 3$ are the baroclinic modes. Minimizing the mean squared error by solving

$$\frac{\partial \varepsilon}{\partial A_n} = 0 \qquad n = 0, 1, 2, 3 \tag{4}$$

results in a set of linear algebraic equations for the A_n which were solved using the successive overrelaxation (SOR) method. The complex coefficients A_n of the north and east components of tidal velocity for each mode were multiplied by their respective real valued eigenfunctions $F_n'(z_i)$ and then combined to obtain the tidal velocity hodographs for each mode. These are shown by month in Figures 5*a* and 5*b* for the depths of 277 m and 2127 m, respectively. The barotropic mode is essentially constant over the water column, while the baroclinic modes vary as in Figure 4. The modal hodographs at all other depths can therefore be obtained by comparing Figure 5 with Figure 4. At these two particular depths, the barotropic mode dominates over the baroclinic modes in which energy is nearly equally distributed. Also the barotropic mode is observed to

TABLE 2. Eigenvalues and Corresponding Horizontal Wavelength for the First Three Baroclinic Modes

n	C_n, m/s	λ_n, km
1	2.35	105
2	1.27	57
3	0.86	39

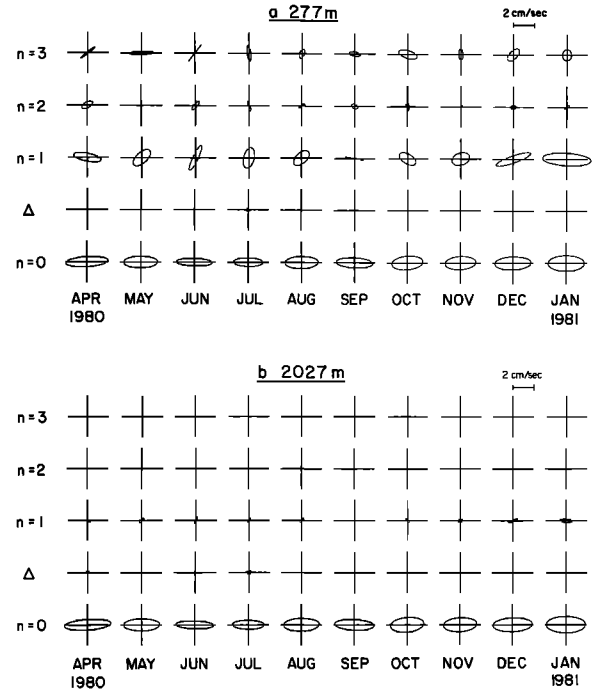

Fig. 5. M_2 tidal current ellipses for the barotropic and the first three baroclinic modes calculated by month over the 10-month sampline interval (*a*) at 727 m and (*b*) at 2127 m. Also shown is the difference Δ each month between the barotropic mode ellipse of that month and the mean barotropic mode ellipse over the 10 months.

be nearly time invariant, while all of the baroclinic modes show considerable variations from month to month. Given that the barotropic mode should be time invariant since it is deterministically forced by the lunar semidiurnal tidal potential, deviations from the mean barotropic M_2 tidal current ellipse may be associated with the stochastic noise within this frequency range. In Figure 5 the set of hodographs immediately above the barotropic mode gives the deviations of the barotropic ellipse of that month from the mean ellipse over the 10 months. The baroclinic mode ellipses must be at least this large in order for them to be at all meaningful. While they do exceed the barotropic mode deviations, the baroclinic modes all appear to be quite random in amplitude, orientation, and phase.

Confidence intervals on the barotropic M_2 tidal current ellipse may be estimated from the rms deviations observed over the 10 independent monthly samples. Figure 6 shows the semimajor axis, semiminor axis, orientation, and phase for the barotropic M_2 tidal current ellipses as functions of time over the 10 months along with their mean values and rms deviations. Assuming that the deviations from the mean ellipse are Gaussian, Table 3 lists the 95% confidence intervals for random errors using a Student's t test. The resulting mean barotropic M_2 tidal current ellipse, its phase relative to the lunar transit at the Greenwich meridian, and its area of uncertainty as determined from the modal fits to 10 months of data are summarized in Figure 7.

The horizontal kinetic energy ratios between each of the individual modes and their sum are given in Table 4. The barotropic mode clearly dominates over the baroclinic modes during all of the 10 months, with the mean barotropic mode percentage being 78.8%. This partition between barotropic and baroclinic tidal energy is midway between the values shown by *Wunsch* [1975], where the internal tide energy had

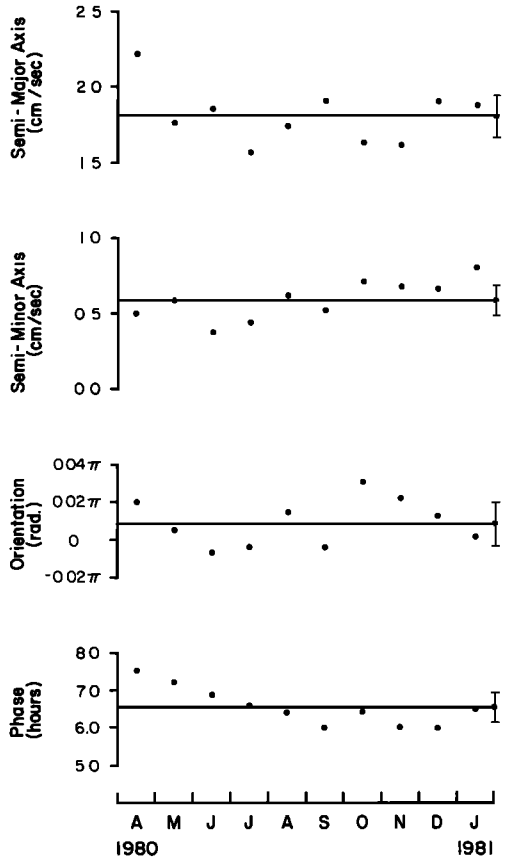

Fig. 6. Semimajor axis, semiminor axis, orientation, and phase (relative to lunar transit of the Greenwich meridian) for the barotropic M_2 tidal current ellipse as a function of time over the 10-month sampling interval along with the means and standard deviations over the 10 months.

between 10 and 50% of the energy of the surface tide at the locations tabulated. Integrating the horizontal kinetic energy density for the mean barotropic M_2 tidal current ellipse over the water column here results in a value for the horizontal kinetic energy per unit area of 6.9×10^5 ergs/cm^2. None of the three baroclinic modes appear to dominate over the others as their percentages vary from month to month.

4. Summary and Discussion

An M_2 tidal current analysis was performed using 10 months of current meter data collected in the eastern Pacific Ocean near 0° near 110°W. A kinematical description of the M_2 tidal current ellipses computed by month at each of 10 depths distributed over the water column from 20 m to 3027 m was presented, and these data were then fit to the barotropic and the first three baroclinic modes determined from a mean buoyancy frequency profile. The principal finding was a robust barotropic M_2 tidal current ellipse which remained very stable in semimajor axis, semiminor axis, orientation, and phase over the 10 months. This is contrasted to the baroclinic tidal currents that were random, isotropic, and without modal preference.

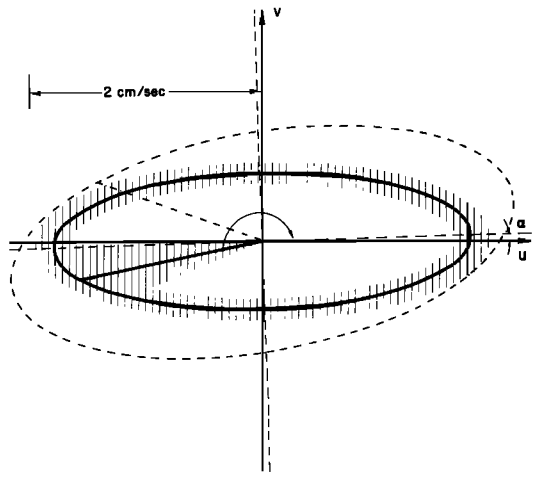

Fig. 7. The mean barotropic M_2 tidal current ellipse, its phase relative to the lunar transit of the Greenwich meridian, and its area of uncertainty using a Student's t distribution with 10 degrees of freedom at the 95% confidence level. Also shown using a dash-dot line is the global tidal model result of E. W. Schwiderski (personal communication, 1986).

The barotropic M_2 tidal current ellipse may be compared with those predicted by numerical solutions to the Laplace tidal equations. *Pekeris and Accad* [1969] present a global distribution of such tidal current ellipses. The 0°, 110°W site in their Figure 12 lies in a region of spatial variability due to the proximity of three amphidromic points. While they do not show an ellipse at this specific location, the results of the analysis given here falls in between those at their adjacent points. The more recent global tidal model of *Schwiderski* [1980] does provide a comparison within $\frac{1}{2}$° of our measurement site. The ellipse calculated from the model (E. W. Schwiderski, personal communication, 1986) is shown along with our results in Figure 7. The model and data compare well. While the modeled amplitudes are larger, the orientation and phase relative the ranges of 180° and 12.42 hours are within 4% and 16% respectively.

The results for the baroclinic tidal currents are qualitatively similar to modal analyses performed for deep ocean stations by others. For example, the baroclinic tidal currents analyzed

TABLE 3. The Parameters of the Mean Barotropic M_2 Tidal Current Ellipse, Their Standard Deviations, and Their 95% Confidence Intervals Based on a Student's t Distribution With 10 Degrees of Freedom

Parameter	Mean	Standard Deviation	Confidence Interval
Semimajor axis, cm/s	1.81	0.19	1.81 ± 0.14
Semiminor axis, cm/s	0.59	0.13	0.59 ± 0.09
Orientation, rad	0.03	0.05	0.03 ± 0.04
Phase, hours	6.56	0.53	6.56 ± 0.38

TABLE 4. Percentages for the Horizontal Kinetic Energy per Unit Area of a Given Mode, $n = 0, 1, 2, 3$, Relative to the Sum of the Four Modes by Month

	$n = 0$	$n = 1$	$n = 2$	$n = 3$
April 1980	79.1	6.5	8.0	6.4
May 1980	74.0	6.3	5.8	13.9
June 1980	74.0	8.2	7.3	10.4
July 1980	73.9	8.1	9.5	8.5
Aug. 1980	86.2	6.2	4.2	3.4
Sept. 1980	87.6	4.2	4.5	3.8
Oct. 1980	77.0	5.6	5.1	12.3
Nov. 1980	86.6	7.0	1.5	4.9
Dec. 1980	77.7	13.7	2.2	6.4
Jan. 1981	71.7	22.0	2.2	4.0

over two separate months by *Magaard and McKee* [1973] were markedly different. This may be due in part to variations in density stratification. However, this would not alter the modal projections as much as was observed, nor would it alter their ellipse orientation and eccentricity. Other aspects of the nonhomogeneous medium through which the baroclinic tidal current energy propagates from its source region must also be important.

In summary, the analyses presented here add an additional data point to the very limited abyssal ocean data set on the global distribution of the barotropic M_2 tidal current. The fact that the baroclinic tidal currents are so random in all of their parameters relative to the deterministically forced and stable barotropic tidal currents remains an interesting topic for investigation.

Acknowledgments. This research was largely supported by the Equatorial Pacific Ocean Climate Studies Project of NOAA. Partial support was also provided by the Oceanography Section, National Science Foundation under grants OCE-8211848 and OCE-8515869. E. W. Schwiderski kindly provided the modelled tidal ellipse shown in Figure 7.

REFERENCES

Gould, W. J., and W. D. McKee, Vertical structure of semidiurnal tidal currents in the Bay of Biscay, *Nature*, *244*, 88–91, 1973.

Halpern, D., and R. D. Pillsbury, Near-surface moored current meter measurements, *Mar. Technol. Soc. J.*, *10*, 31–38, 1976.

Hendershott, M. C., Numerical models of ocean tides, in *The Sea*, vol. 6, edited by E. D. Goldberg et al., pp. 47–95, Interscience, New York, 1975.

Hendershott, M. C., Long waves and ocean tides, in *Evolution of Physical Oceanography*, edited by B. A. Warren and C. Wunsch, pp. 292–341, MIT Press, Cambridge, Mass., 1981.

Hendry, R., Observations of the semidiurnal internal tide in the western northern Atlantic Ocean, *Philos. Trans. Roy. Soc. London, Ser. A*, *286*, 1–24, 1977.

Magaard, L., and W. D. McKee, Semi-diurnal tidal currents at site D, *Deep Sea Res.*, *20*, 997–1010, 1973.

Munk, W., F. Snodgrass, and M. Wimbush, Tides off-shore: Transition from California coastal to deep sea waters, *Geophys. Fluid Dyn.*, *1*, 161–235, 1970.

Pekeris, C. L., and Y. Accad, Solution of Laplace's equation for the M_2 tide in the world oceans, *Philos. Trans. Roy. Soc. London, Ser. A*, *265*, 413–436, 1969.

Schott, F., and J. Willebrand, On the determination of internal wave direction spectra from moored instruments, *J. Mar. Res.*, *31*, 116–134, 1973.

Schwiderski, E. W., Ocean tides II: A hydrodynamic interpolation model, *Mar. Geod.*, *3*, 219–255, 1980.

Wunsch, C., Internal tides in the ocean, *Rev. Geophys.*, *13*, 167–182, 1975.

D. Halpern, Jet Propulsion Laboratory, California Institute of Technology, Pasadena, CA 91109.

S. M. Hwang, Cooperative Institute for Marine and Atmospheric Studies, Rosenstiel School for Marine and Atmospheric Science, University of Miami, 4600 Rickenbacker Causeway, Miami, FL 33149.

T. Y. Tang and R. H. Weisberg, Department of Marine Science, University of South Florida, 140 7th Avenue South, Saint Petersburg, FL 33701.

(Received June 9, 1986;
accepted September 9, 1986.)